

Electronic Supplementary Information

Tuning selectivity of CO₂ hydrogenation using ceramic hollow fiber catalytic modules

Shunottara M Jogdand^{a,d}, Prachiti R Bedadur^b, Arun Torris^b, Ulhas K Kharul^{b,d}, V. Satyam

Naidu^{c,d,}, R. Nandini Devja^{a,d,*}*

^aCatalysis and Inorganic Chemistry Division, ^bPolymer Science and Engineering Division,

^cChemical Engineering and Process Development Division, CSIR-National Chemical

Laboratory, Pune 411008, ^dAcademy of Scientific and Innovative Research (AcSIR), Ghaziabad-

201002, India

E-mail: nr.devi@ncl.res.in, Phone No.: +9120 25902271; sn.vasireddy@ncl.res.in, Phone No.:

+912025902952.

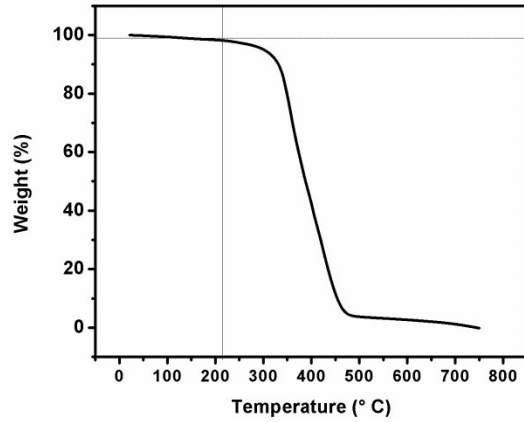


Figure S1. Thermogravimetric analysis of the epoxy glue used for module making

[S2a] Permeability method using bubble point assembly

The complete wetting of pores present in the modulated single AHF was performed by immersing the complete module in a wetting liquid i.e., deionized water for 24 h. The wetting liquid (water), saturated in the wetted pores was then displaced by the iso-butyl alcohol (IBA, 23.0 dynes/cm at 20 °C) having low surface tension than that of water (72.8 dynes/cm at 20 °C) along with immiscibility. The shell side pressure was varied gradually to displace water by the IBA hence can obey the Laplace equation (1). The calculated interfacial tension of water/IBA is 1.85 mN/m at 25 °C. The relationship between pressure and pore radius is given by the Laplace equation,

$$r = \frac{2\gamma \cos \theta}{p_i - \Delta P} \quad (1)$$

Where, r_{pi} is the radius of a capillary shaped pore and γ the surface tension at the liquid-liquid interface. θ is the angle between solid/liquid interfaces. The pores with largest pore size resulting in flux can be described by the Hagen-Poiseuille equation (2),

$$n_i = \left(J_i - \frac{J_{i-1} P_i}{P_{i-1}} \right) \frac{8l\eta}{\pi p_i r_{pi}^4} \quad (2)$$

Where, J is the flux at pressure P . η is the viscosity of IBA and l is the thickness of the wall of the AHF. Water will be displaced from the larger pores initially, which can be collected as flux using volumetric flow meter. Increasing the pressure causes the water in smaller pores to be displaced thus increasing the flux through the wall and water flux was obtained as a function of the pore radius and from the curve, the pore size distribution can be calculated.¹

The pore with largest area can be calculated by connecting the same module to the bubble point assembly²⁻³ where the water in the largest pore will be displaced by air at a particular pressure. An air bubble will penetrate through the pore when the radius of the bubble is equal to that of pore radius.

[S2b] Determination of Porosity Using Micro-tomography Imaging

The resultant 3D reconstructed model was used to estimate the pore characteristics such a percentage porosity, specific surface area (m^2/m^3) etc., using PoroDict® software package where pore diameter was determined by fitting spheres into the pore volume. For Percentage porosity (%) calculations, AHFs were scanned at a specific pixel size during X-ray microtomography imaging process and the size depends upon the resolution. Scanned virtual cross sectional images were subjected to image processing technique called segmentation, where pixels / voxels pertaining to pore space was differentiated. During this process, porosity was calculated, which was defined as the total pore volume divided by the total sample volume.

$$\text{Porosity (\%)} = \frac{\text{Pore Volume}}{\text{Total Volume}} \times 100$$

The algorithm used for the estimation of specific (pore) surface area calculates an approximation of the surface area by statistical methods. To determine the surface area, the Crofton formula⁴ is used, which relates at first the 3D surface area to an integral over 2D boundary lengths of planar cross sections and then second these lengths to an integral over 1D rays. Based on this formula, an analysis of the intersection points of rays in all space directions with the structure allows determining the surface area. The surface area; $1.83705 \times 10^{-6} \text{ m}^2$ and specific surface area; $4.3508 \times 10^4 \text{ m}^2/\text{m}^3$ of segmented image was calculated.

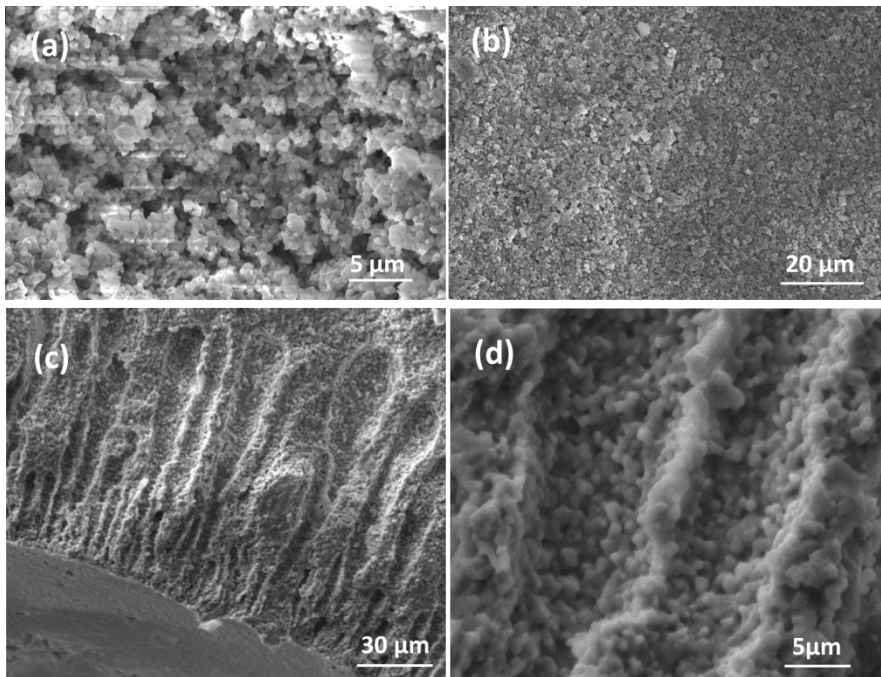


Figure S3. SEM imaging of (a) inner and (b) outer wall surface along with (c) and (d) the figure like structure showing porous nature of the AHF calcined at 1500 °C

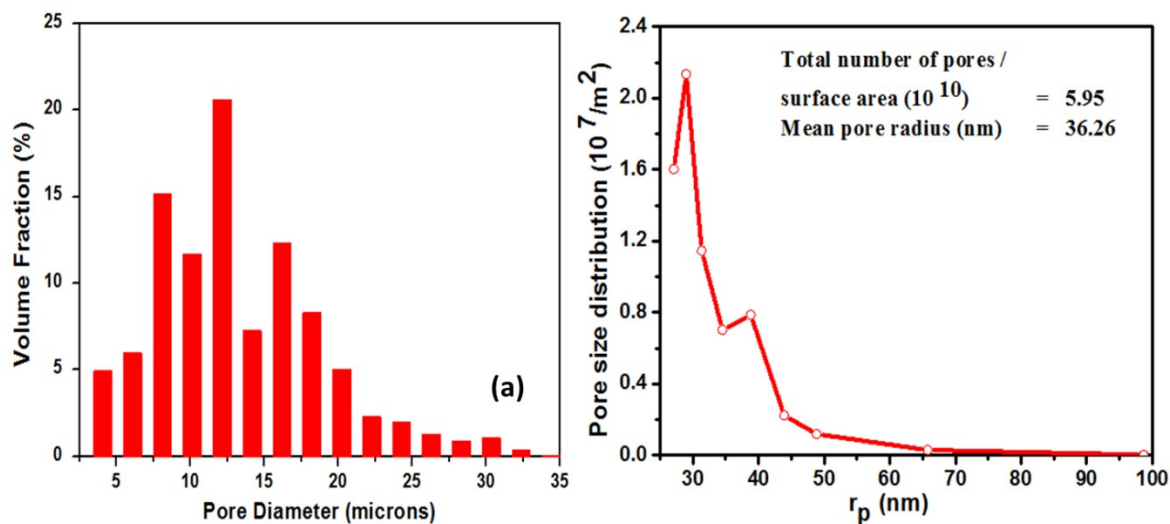


Figure S4. Histogram of pore-size distribution in AHFs by (a) tomography and (b) permeability analysis

Table S5. Nitrogen sorption studies

catalyst	AHF	5N-AHF
BJH method		
BET (m ² /g)	0.8089± 0.4	1.603± 0.4
* Surface area (m ² /g)	0.4906± 0.4	1.259± 0.4
* Pore volume (mL/g)	0.0069± 0.04	0.0238± 0.04
* Pore size (nm)	5.391± 1	4.851± 1

*measurements at the adsorption-desorption point

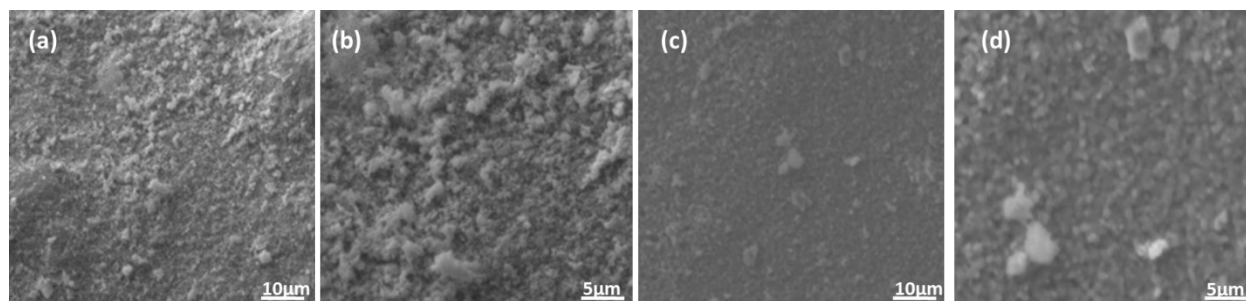


Figure S6. E-SEM images of the higher metal (6.5 wt. %) loaded AHFs with (a), (b) Outer wall, (c) and (d) Inner wall

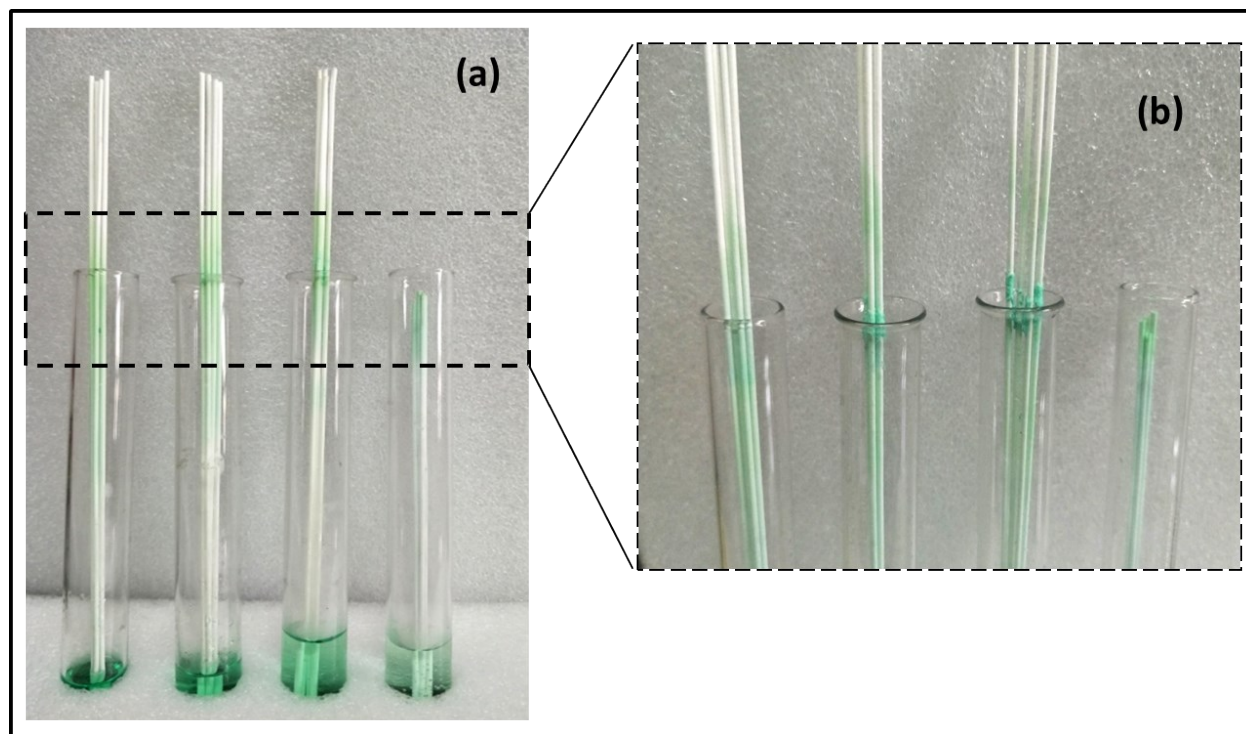


Figure S7. (a) Effect of dilution of the 5 wt. % (2 mL, 4 mL, 6 mL respectively) Ni salt solution and the effect of the length (with 6 mL dilution) of the AHFs impregnated by capillary action rise method, where (b) agglomeration of the salt at the walls of the AHFs were observed

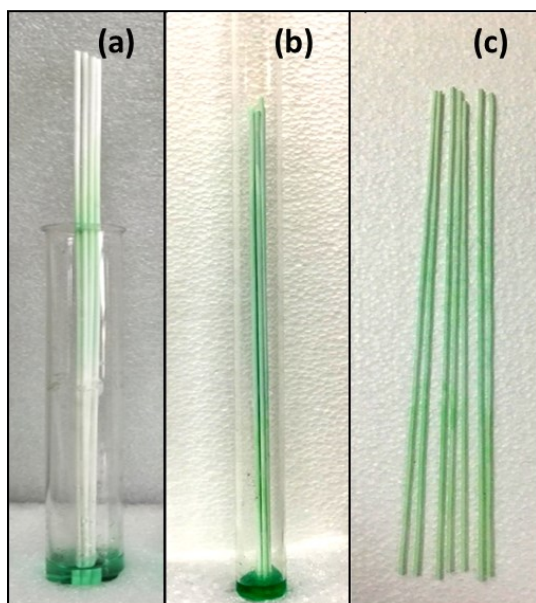


Figure S8: The images of (a) open and (b) closed system for capillary rise method along with the uniformly deposited Ni-AHF's obtained by closed system

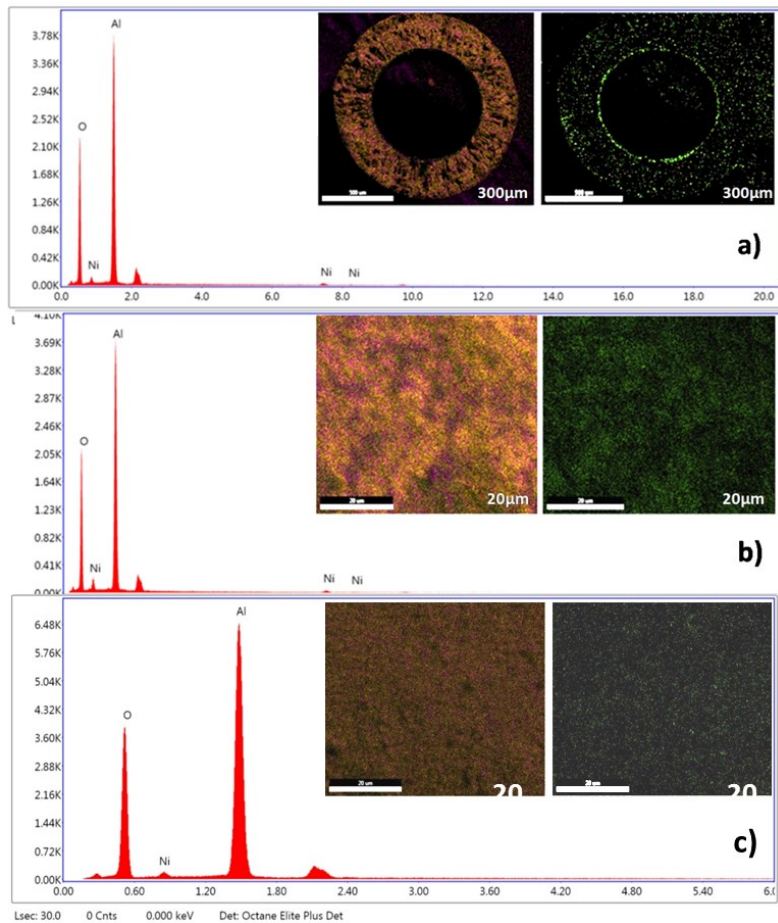


Figure S9. E-mapping of the 5N-AHF a) cross-section (scale bar 300 μm), b) outer wall and c) inner wall (scale bar 20 μm) along with the EDAX reports where the report shows presence of 5 wt. % of Ni

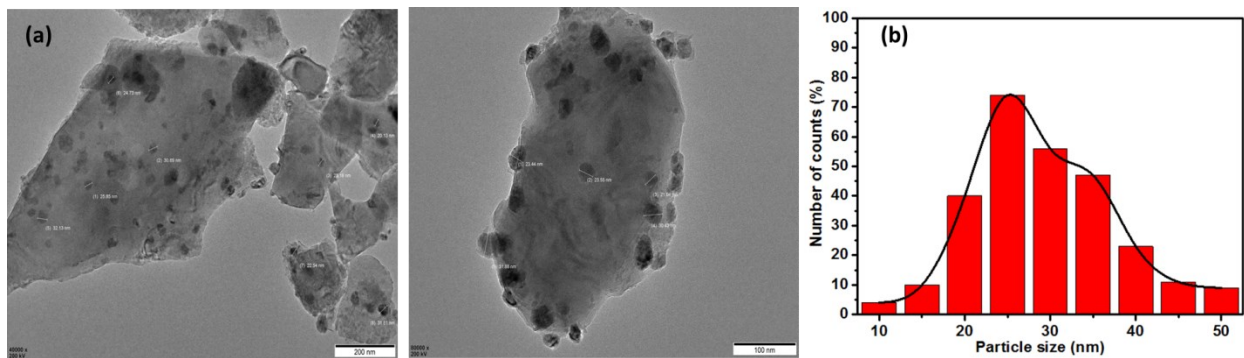


Figure S10. (a) HR-TEM images with the dimensions of particle size and (b) its histogram of the Ni metal present in the Ni/AHFs catalyst

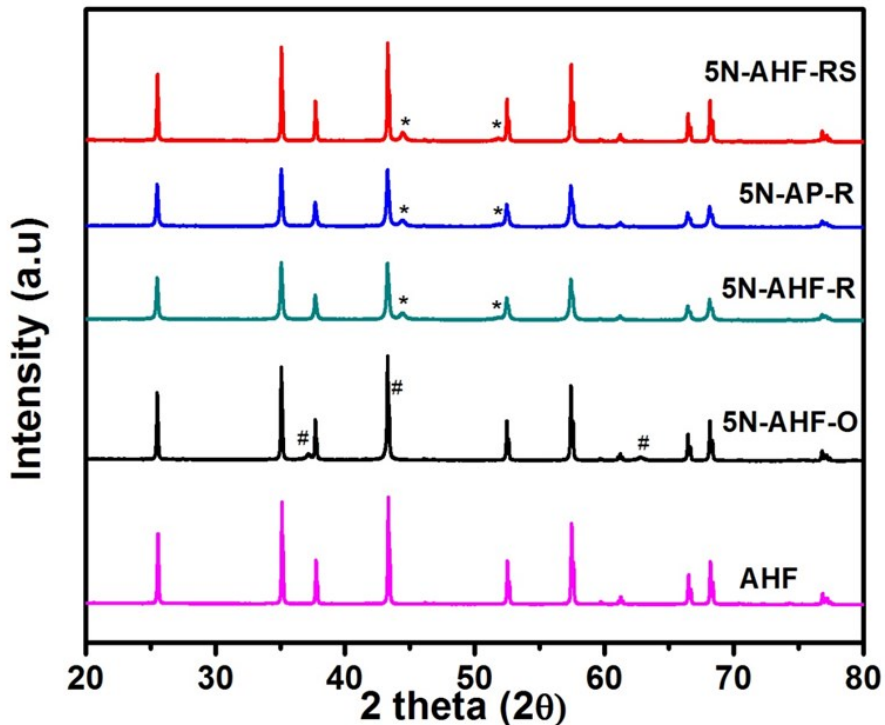


Figure S11. Powder X ray diffraction analysis (PXRD) of crushed AHFs (AHF), fresh Ni/AHF (5NAHF-O_{calined}, 5N-AHF-R_{reduced}, 5N-AP-R_{reduced}) catalyst and Spent (5N-AHF-RS) catalyst (NiO[#] and Ni^{*})

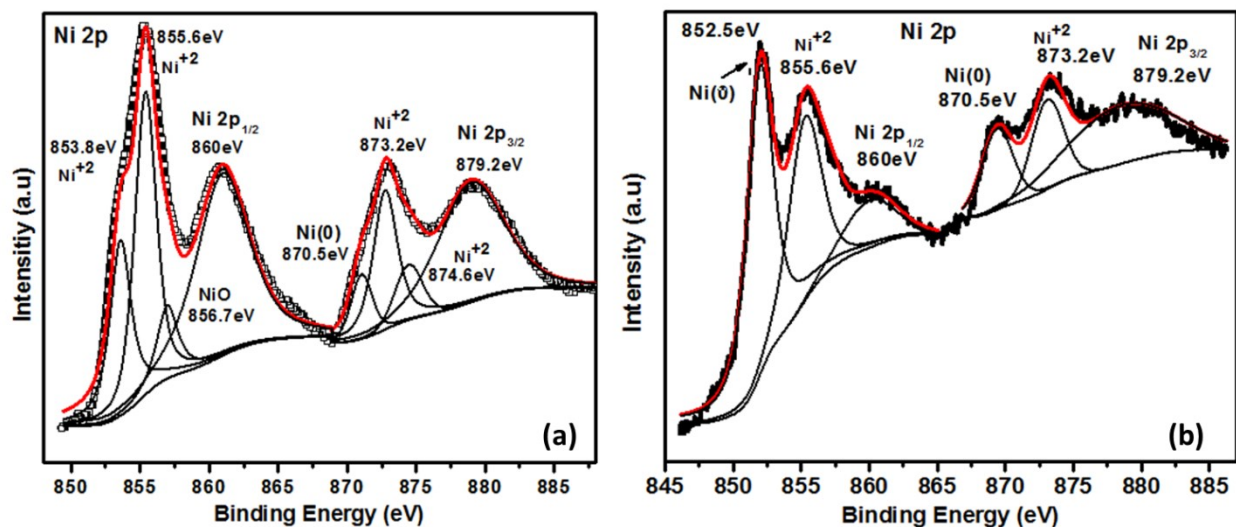


Figure S12. X-ray photoelectron spectroscopy (XPS) of (a) Fresh (5N-AHF-O) catalyst and (b) Fresh reduced (5N-AHF-R) catalyst respectively

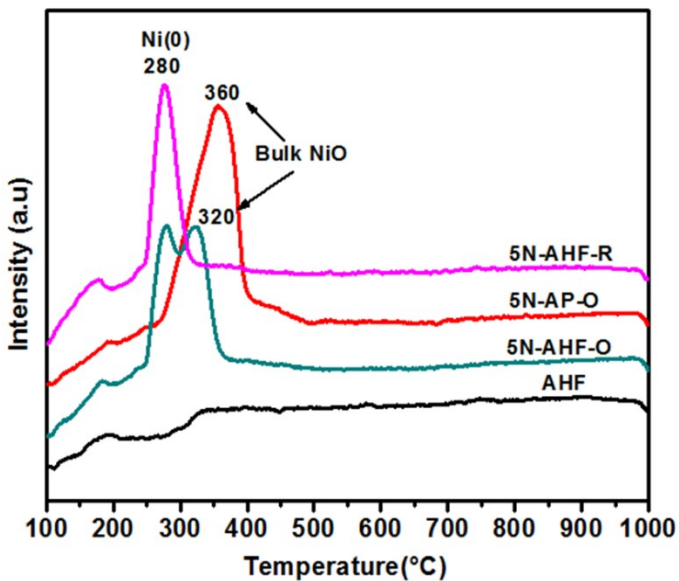


Figure S13. H₂-TPR of alumina (AHF) and AHF fresh catalysts; calcined (5N-AHF-O, 5N-AP-O) and reduced (5N-AHF-R) respectively

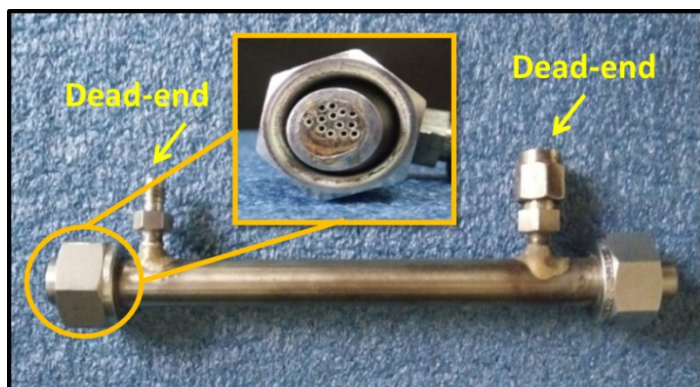


Figure S14. NiO/AHF's modulation in SS reactor with the help of Epoxy glue

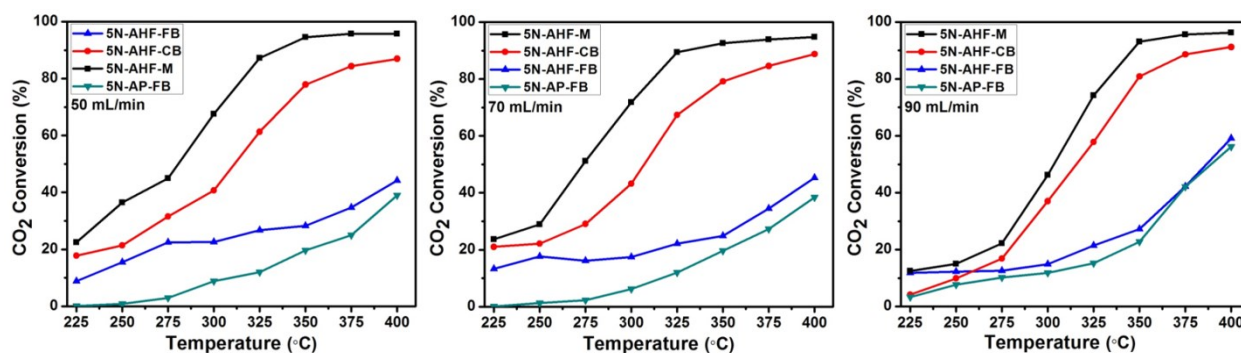


Figure S15. The percentage CO₂ conversion as a function of temperature for (□) model (a); Modulated (5N-AHF-M) catalyst, (○) model (b); (5N-AHF-CB) complete bed packing (5NAHF-B) catalyst, (Δ) model (c); fixed bed packing (5N-AHF-FB) catalyst, (□) model (d); fixed bed packing powder (5N-AP-FB) catalyst for the flow rates 50, 70 and 90 mL.min⁻¹, respectively

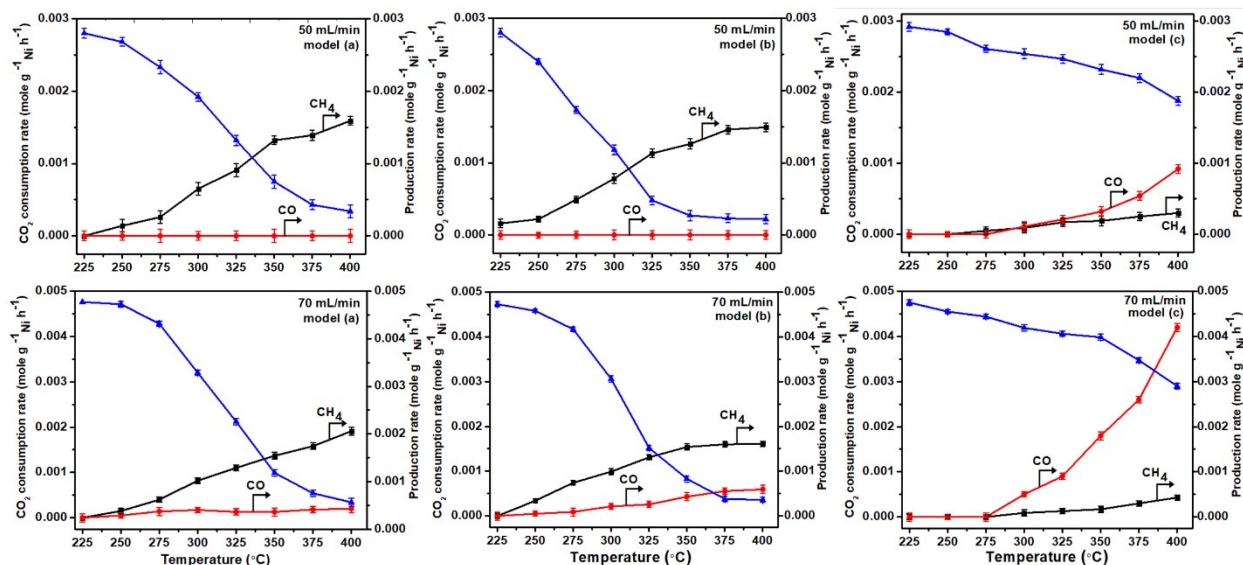


Figure S16. The graph of concentration of unreacted CO₂ (Δ, blue), CH₄ (□, black) and CO (○, red) in the outlet per gram of metal (Ni) with respect to temperature for model (a); modulated (5NAHF-M) catalyst, model (b); complete bed packing (5N-AHF-CB) catalyst and model (c); fixed bed packing (5N-AHF-FB) catalyst for the flow rates (a) 50 mL.min⁻¹ and 70 mL.min⁻¹, respectively

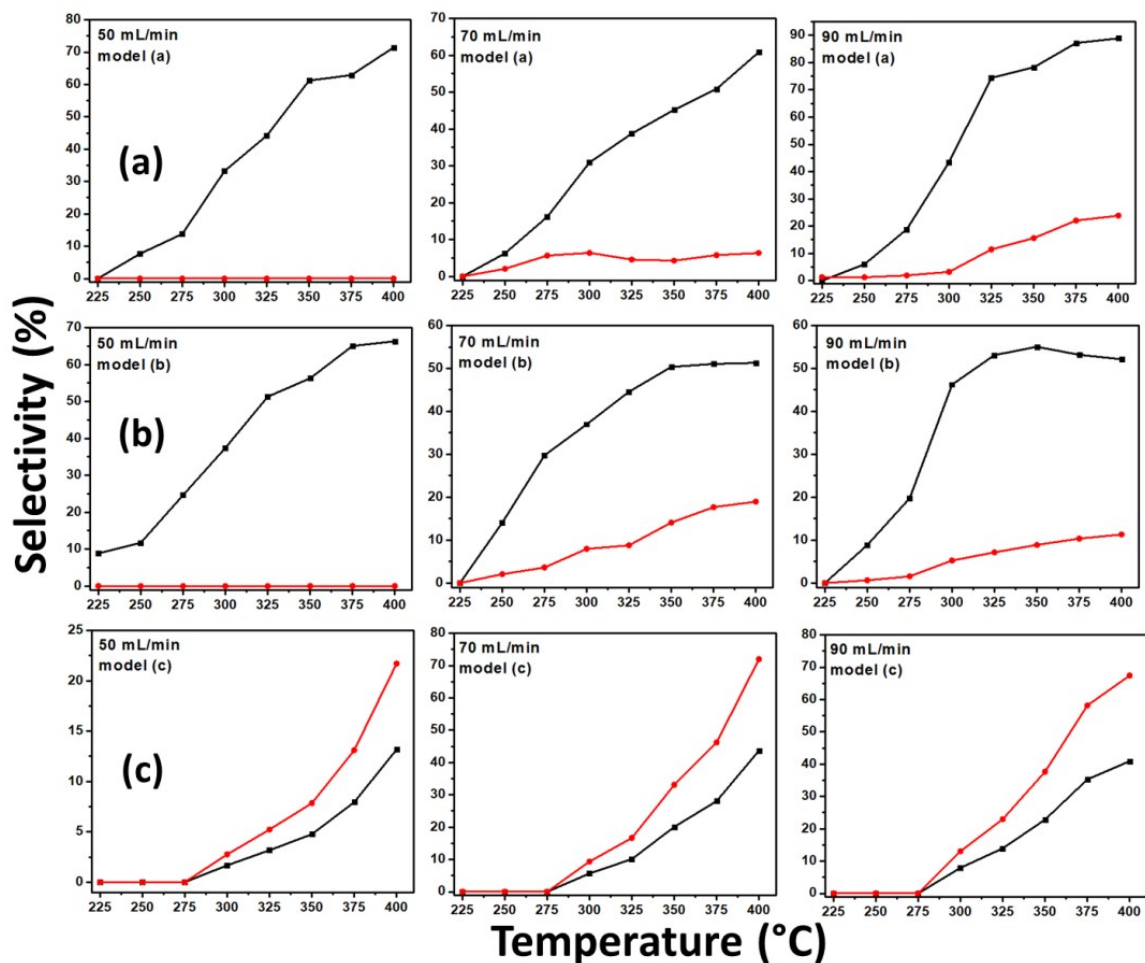


Figure S17. The graph selectivity of CH₄ (□, black) and CO (○, red) over the reacted CO₂ at different temperature for model (a); modulated (5NAHF-M) catalyst, model (b); complete bed packing (5N-AHF-CB) catalyst and model (c); fixed bed packing (5N-AHF-FB) catalyst for the flow rates 50 mL.min⁻¹, 70 mL.min⁻¹ and 90 mL.min⁻¹, respectively

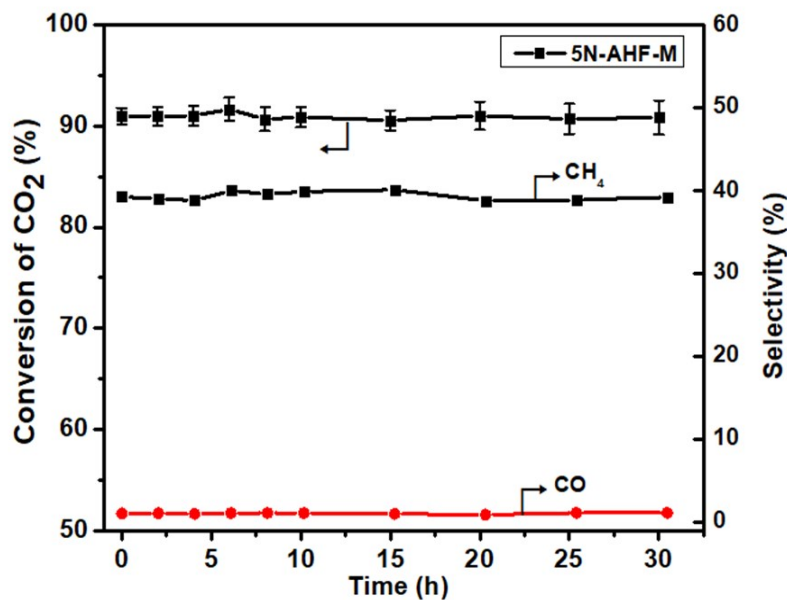


Figure S18. The conversion of CO₂ (□, black) and selectivity of CH₄ (□, black) and CO (○, red) for model (a); (5N-AHF-M) at 350°C for 30h with the flow rate 90 mL.min⁻¹

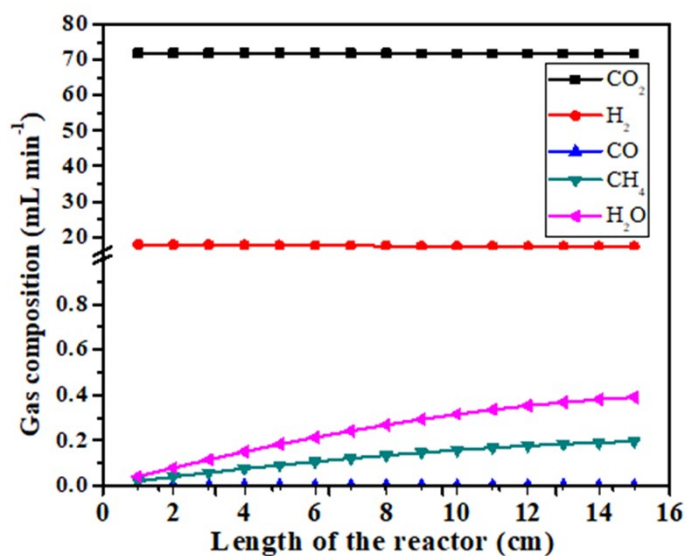


Figure S19. The concentration of the gases along the length of the reactor is simulated using MATLAB code at isothermal temperature of 400°C for model (a).

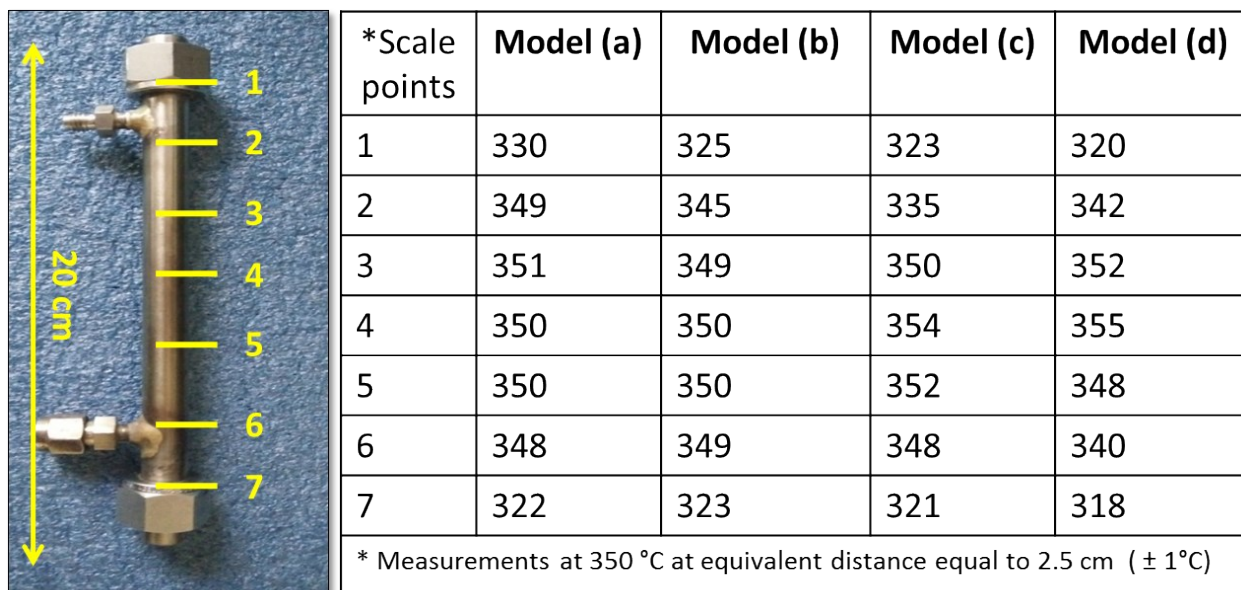


Figure S20. The external thermal profiling of the reactor during the reaction at 350°C for all the models (a), (b), (c) and (d) respectively

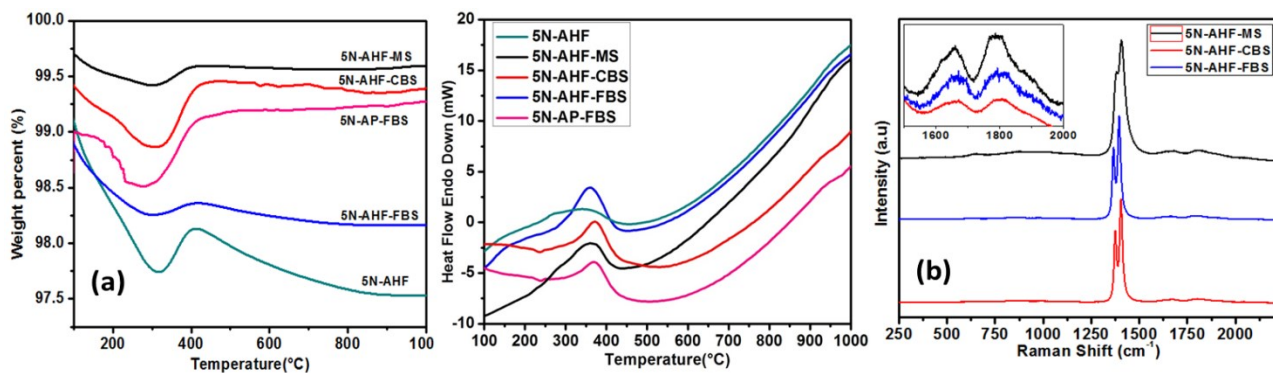


Figure S21. (a) Thermo-gravimetric Analysis (TGA) of Fresh (5N-AHF) and spent (5N-AHF-MS, 5N-AHF-CBS, 5N-AHF-FBS) catalyst and (b) Raman shift for spent catalyst with model (a) 5NAHF-MS, (black), (b) 5N-AHF-CBS (red) and (c) 5N-AHF-FBS (blue) respectively

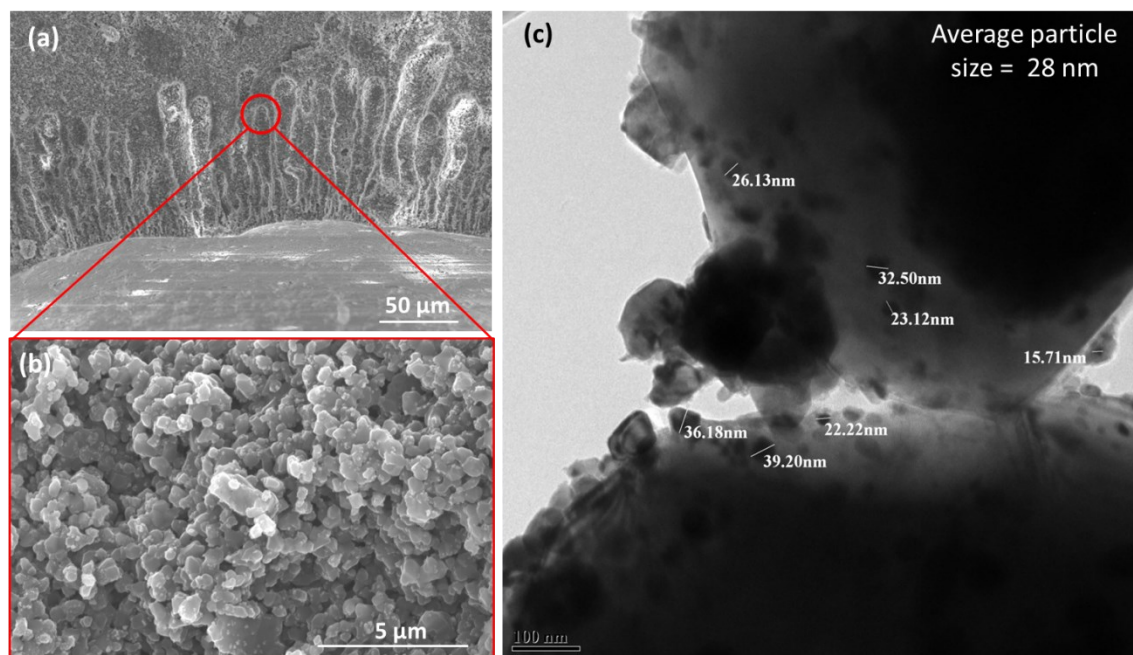


Figure S22. (a and b) SEM and HR-TEM analysis of spent Ni/AHF catalyst used in model (a); (5N-AHF-M) at 350°C for 30h with the flow rate 90 mL.min⁻¹

[S 23] Equilibrium, rate constants and adsorption coefficients for three reactions at 400 °C

Table 1. Equilibrium constants for three reactions at 400 °C

Equilibrium constant	Quantity
K ₁	5.24E-05
K ₂	10.8404
K ₃	5.68E-04

Table 2. Rate constants for three reactions at 400 °C

Parameter	Forward rate constant	Reverse rate constant
k ₁ (mol/s. bar.)	2.71E-04	0.19

kg cat)		
k_2 (mol/s. bar. kg cat)	3.3446	3.24
k_3 (mol/s. bar. kg cat)	3.32E-05	17.12

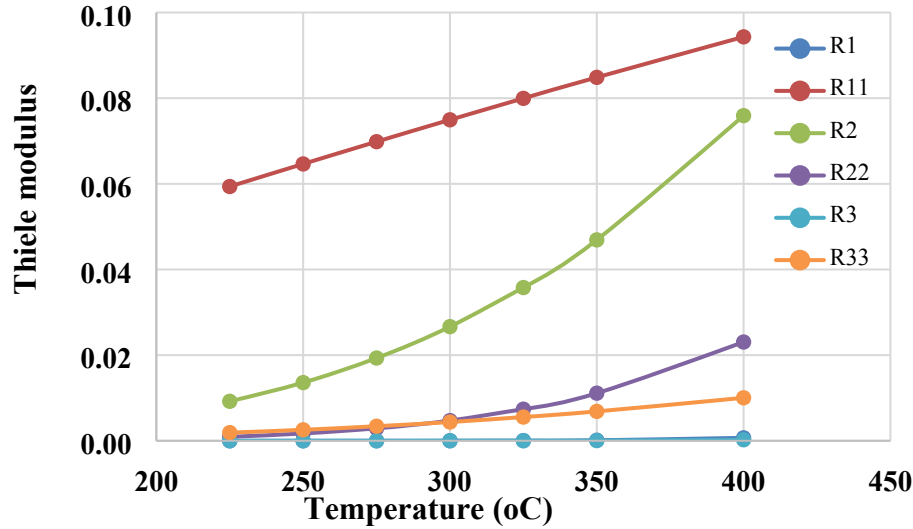
Rate constants ratio	Factor
$k_{1,f}/k_{3,f}$	8.15
$k_{3,r}/k_{1,r}$	88.39

Table 3. Adsorption coefficients for three reactions at 400 °C

Adsorption constants	Quantity
K_{CO} (bar ⁻¹)	25.0652
K_{CH4} (bar ⁻¹)	0.6223
K_{H2} (bar ⁻¹)	0.0232
K_{H2O} (bar ⁻¹)	0.0166

Equilibrium constant ratio	Quantity
K_{CO}/K_{CH4}	40.28
K_{CO}/K_{H2}	1080.40
K_{CO}/K_{H2O}	1509.95

[S 24] Variation of Thiele modulus (forward reaction, R1, R2, R3 and reverse reaction, R11, R22, R33) with temperature



REFERENCES

1. J. Zhao, J. Y. Chong, L. Shi and R. Wang, J. Membr. Sci., 2019, **572**, 210.
2. Mulder, M., Basic Principles of Membrane Technology **1996**: Netherlands.
3. E. Jakobs and W. J. Koros, W. J. J. Membr. Sci., 1997, **124**, 149.
4. J. Ohser and F. Mücklich, Statistical Analysis of Microstructures in Materials Science, Wiley and Sons, 2000, 115.